EPJ Web of Conferences **359**, 01016 (2026) https://doi.org/10.1051/epjconf/202635901016
ICEMR-2025

Systematic Tuning of Electronic Band Gap with Varying Dopant Concentration in Zinc Gallate Nanoparticles

Soundar R[1&2], *Manjunatha* H.C[3,*], *Upendra Kumar* Kagola[2,**], *Muniratnam* R[4], and *Vishwalinga Prasad* B[1,]

[1]Department of Physics, Government College for women, Kolar-563101, Karnataka, India
[2]Department of Physics, School of Applied Sciences, REVA University, Bengaluru - 560064, Karnataka, India
[3]Department of Physics, Government First Grade College, Devanahalli-562110, Karnataka, India
[4]Department of Physics, Rajah Serfoji Government College, Thanjavur-613005, Affiliated to Bharathidasan University, Tiruchirappalli-TamilNadu,India

Abstract.

Rare-earth (RE^{3+} = Eu^{3+}, Tb^{3+}, Sm^{3+}, and Er^{3+}) doped $ZnGa_2O_4$ nanoparticles were synthesized using an eco-friendly aloe vera-assisted green combustion method. The rapid exothermic reaction produced fine nanocrystalline powders, which were subsequently calcined at 600^0C for improved crystallinity. PXRD confirmed the formation of a pure cubic spinel phase with no impurity peaks, while slight peak shifts and broadening indicated the presence of lattice strain and nanoscale crystallite dimensions. The combustion-derived powders exhibited agglomerated, irregular morphologies typical of gas-evolving reactions. Optical diffuse reflectance spectroscopy revealed a clear dependence of the energy band gap (Eg) on both crystallite size and dopant concentration. For all RE dopants, the Eg decreased progressively with increasing particle size, reflecting the relaxation of quantum-confinement effects. Similarly, Eg showed a systematic decrease with higher dopant mol%, attributed to dopant-induced lattice distortion, creation of defect states, and modification of local electronic environments within the $ZnGa_2O_4$ matrix. Among the dopants, Er^{3+} exhibited the highest Eg in the undoped limit, while Tb^{3+} produced the strongest band-gap narrowing at higher concentrations. These results demonstrate that RE doping combined with size control offers an effective strategy for tailoring the optical band structure of $ZnGa_2O_4$, underscoring its potential for photonic, sensing, and optoelectronic applications.

1 Introduction

Zinc gallate ($ZnGa_2O_4$) is an important wide band gap semiconductor belonging to the cubic spinel family (space group Fd3m)[2] well known for its excellent chemical stability, high thermal resistance, low toxicity, and remarkable optical transparency in the ultraviolet region[3]. Owing to its large band gap (4.4–4.7 eV in bulk form)[2] and robust structural framework, $ZnGa_2O_4$ has attracted significant attention for applications in phosphors,

*e-mail: manjunathhc@rediffmail.com
**e-mail: rajavaram.ramraghavalu@reva.edu.in

optoelectronic devices, photocatalysis, sensors, and nonlinear optical systems[4]. At the nanoscale, its optical and electronic properties can be further modified through size confinement effects and defect engineering[5], making $ZnGa_2O_4$ nanoparticles particularly promising for tunable photonic applications.

Rare-earth (RE^{3+}) ion doping is an effective strategy to tailor the structural and optical properties of wide band gap oxides[6]. The partially filled 4f electronic configuration of RE^{3+} ions gives rise to sharp intra-4f transitions, long-lived excited states, and unique luminescence characteristics[7]. When incorporated into host lattices, RE^{3+} ions can introduce localized impurity levels within the forbidden gap, modify the local crystal field environment, and induce lattice strain due to ionic radius mismatch[8]. These effects often lead to band gap modulation, enhanced light absorption, and defect-assisted electronic transitions. In particular, RE-doped $ZnGa_2O_4$ systems have demonstrated promising performance in phosphorescent, sensing, and energy-related applications, where controlled band gap tuning is crucial[9].

However, despite the extensive research on rare-earth-doped $ZnGa_2O_4$ nanomaterials, systematic studies establishing a direct correlation between dopant concentration, crystallite size, and optical band gap modulation remain limited. In particular, understanding how rare-earth ions influence the electronic structure through lattice distortion, defect generation, and microstructural evolution is still an important challenge. Therefore, the present study aims to investigate the influence of different rare-earth dopants and their concentration on the structural parameters and optical band gap behavior of $ZnGa_2O_4$ nanoparticles synthesized via an eco-friendly aloe-vera-assisted combustion method. In recent years, green synthesis approaches have gained increasing importance due to environmental concerns and the need for sustainable material processing[10]. Bio-assisted combustion methods employing plant extracts as fuels and chelating agents provide a cost-effective, eco-friendly route for producing nanocrystalline oxides with controlled morphology and high phase purity[10]. However, systematic studies correlating dopant concentration, crystallite size, and electronic band gap evolution in RE^{3+}-doped $ZnGa_2O_4$ nanoparticles remain limited[11]. Therefore, the present work focuses on the synthesis of RE^{3+} = Er^{3+}, Sm^{3+}, Eu^{3+}, and Tb^{3+})-doped $ZnGa_2O_4$ nanoparticles via an aloe-vera-assisted green combustion route and investigates the influence of dopant concentration and crystallite size on structural parameters and optical band gap behavior. The study aims to establish a clear relationship between rare-earth incorporation and band structure engineering for advanced optoelectronic applications.

2 Materials and Methods

Rare-earth (Eu, Tb, Sm, and Er) doped $ZnGa_2O_4$ nanoparticles were prepared through a green combustion synthesis method employing aloe vera extract. Appropriate stoichiometric quantities of zinc nitrate, gallium nitrate, and the corresponding rare-earth nitrate precursors were first dissolved in deionized water. Aloe vera gel was then introduced into the solution, serving simultaneously as a bio-fuel and chelating agent to promote homogeneous mixing and controlled combustion. The mixture was continuously stirred for 1 hour to ensure the formation of a uniform viscous gel. Subsequently, the gel was heated at 500°C to initiate a self-sustained combustion reaction, yielding a fine precursor powder. This as-burnt powder was further calcined at 600°C for 3 hours to obtain the well-crystallized cubic spinel $ZnGa_2O_4$ phase. The final nanopowders exhibited good phase purity and uniform morphology and were subsequently subjected to detailed characterization. The synthesis flowcahrt and mechanism is explained in our previous work [12].

3 Results and Discussions

3.1 PXRD analysis of ZG:RE^{3+} doped NPs

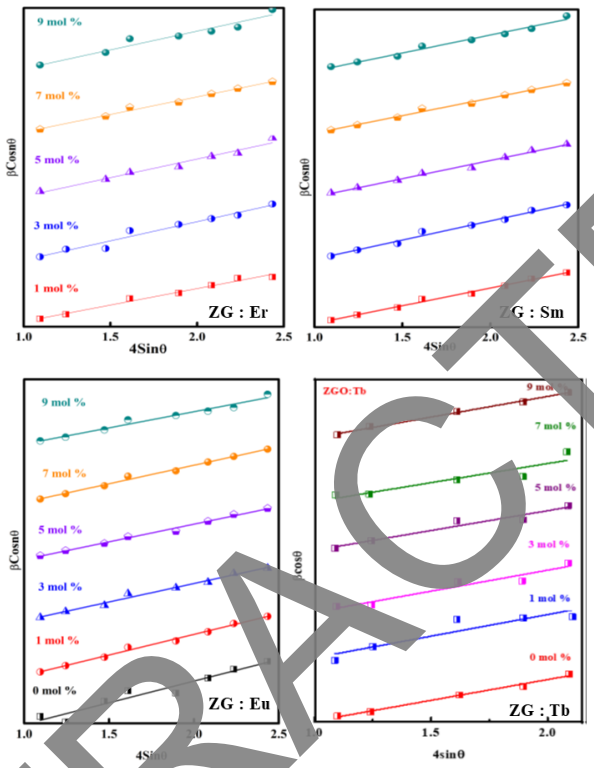

Figure 1. (a-d).Williamson–Hall (β cosθ versus 4sinθ) plots of RE-doped $ZnGa_2O_4$ nanoparticles (1–9 mol%)

The powder X-ray diffraction (PXRD) patterns of rare-earth doped $ZnGa_2O_4$ (ZGO:RE; RE = Sm, Er, Eu, Tb) nanoparticles confirm the formation of a single-phase cubic spinel structure for all compositions. The prominent diffraction peaks indexed to the crystallographic planes (111), (220), (311), (222), (400), (331), (511), (440), and (531) appear at 2θ values of approximately 24.70^0, 31.72^0, 34.47^0, 36.39^0, 43.39^0, 47.66^0, 56.70^0, 63.05^0, and 68.01^0, respectively[13]. These reflections are in good agreement with the standard data for cubic $ZnGa_2O_4$ (space group $Fd\bar{3}m$, JCPDS card No. 86-0415)[12], confirming the retention of the host lattice structure upon doping. Importantly, no additional impurity peaks corresponding to secondary rare-earth oxides or other intermediate phases are detected, indicating successful incorporation of RE^{3+} ions into the $ZnGa_2O_4$ lattice without altering the fundamental crystal symmetry. Furthermore, the peak positions (2θ) and corresponding (hkl) indices remain nearly identical for all doping concentrations (1–9 mol%) and across different rare-earth ions (Sm, Er, Eu, Tb), suggesting minimal lattice distortion and preservation of phase purity.

The Williamson–Hall (W–H) plots constructed for ZGO:RE(Fig1(a-d) samples (β cosθ versus 4sinθ) further substantiate the structural integrity of the doped systems. Linear fitting of the W–H plots for different doping concentrations (1–9 mol%) exhibits good correlation,

indicating that peak broadening arises from the combined contribution of crystallite size and microstrain. The nearly parallel nature of the fitted lines for various dopant concentrations suggests that the intrinsic strain introduced by rare-earth substitution is relatively small and uniformly distributed within the lattice. Since the diffraction peak positions and indexed planes used for W–H analysis are consistent across all samples, the structural framework of cubic $ZnGa_2O_4$ remains unchanged irrespective of dopant type or concentration. The absence of extra reflections in both PXRD patterns and W–H analysis confirms that the rare-earth ions are effectively substituted into the host matrix without phase segregation. Overall, the PXRD and Williamson–Hall results collectively demonstrate high crystallinity, phase stability, and successful rare-earth incorporation in the $ZnGa_2O_4$ spinel structure synthesized via the green combustion route.

3.2 Energy Gap analysis of ZG:RE^{3+} doped NPs

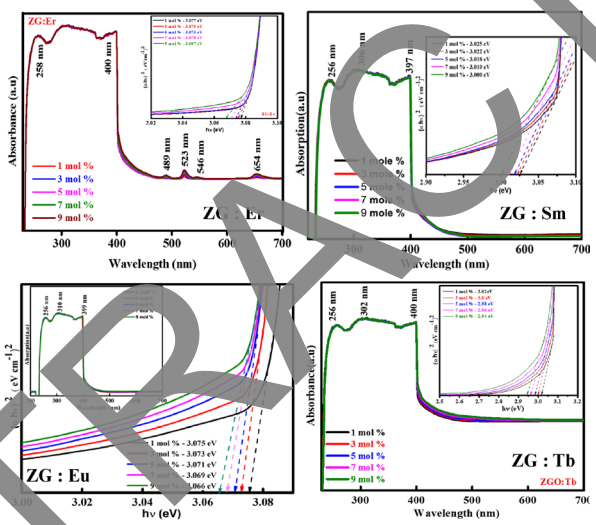

Figure 2. UV–Visible absorption spectra of RE^{3+} = Er^{3+}, Sm^{3+}, Eu^{3+}, and Tb^{3+})-doped ZG samples (1–9 mol%) recorded in the wavelength range of 200–700 nm, along with the corresponding Tauc plots

The UV–Visible absorption spectra of RE^{3+} = Er^{3+}, Sm^{3+}, Eu^{3+}, and Tb^{3+}-doped ZG samples (1–9 mol%)[14](Fig2) exhibit intense absorption in the ultraviolet region ($\lambda < 400$ nm), which is primarily attributed to intrinsic band-to-band transitions of the host lattice along with $O^{2-} \rightarrow RE^{3+}$ charge transfer transitions, confirming strong host–dopant electronic interaction. In the Er^{3+}-doped system, well-resolved absorption bands centered at approximately 258 and 460 nm, along with weaker features around 492, 523, 546, and 654 nm, are assigned to characteristic intra-4f transitions of Er^{3+} ions arising from Stark-split energy levels, indicating successful incorporation of Er^{3+} into the lattice without secondary phase formation. The Sm^{3+}-doped samples display prominent absorption bands near 256, 306, and 397 nm, corresponding to charge transfer and 4f–4f transitions of Sm^{3+}, while maintaining nearly identical spectral profiles across concentrations, suggesting structural stability upon doping. Similarly, Eu^{3+} and Tb^{3+} incorporation introduces identifiable visible-region absorption features associated with their respective 4f electronic transitions, superimposed on the

strong host absorption edge, further confirming substitutional incorporation into lattice sites. With increasing dopant concentration, a slight enhancement in absorption intensity is observed, which can be attributed to the increased population of RE^{3+} ions and the creation of localized electronic states within the forbidden gap. The optical band gap values were determined using Tauc plots of $(\alpha h\nu)^2$ versus photon energy ($h\nu$), which reveal a linear region characteristic of a direct allowed transition for all compositions. A gradual red shift of the absorption edge and a systematic reduction in band gap energy are observed with increasing RE^{3+} concentration, indicating band gap tuning through dopant-induced modifications in the electronic structure. This band gap narrowing can be ascribed to lattice distortion arising from ionic radius mismatch between host and dopant ions, the formation of defect states and oxygen vacancies, enhanced carrier–phonon interactions, and the introduction of intermediate impurity levels that reduce the effective energy separation between valence and conduction bands. Since the synthesized samples are obtained in powder form, UV–Visible diffuse reflectance spectroscopy (DRS) was employed instead of transmission absorption measurements. The reflectance data were converted into an equivalent absorption function using the Kubelka–Munk relation:

$$F(R) = \frac{(1-R)^2}{2R} \tag{1}$$

where R is the diffuse reflectance. The Kubelka–Munk function F(R) is proportional to the absorption coefficient and was used to construct Tauc plots for band gap estimation. Therefore, the sample thickness parameter required in transmission absorption measurements is not applicable in the present study.

3.3 Energy Gap analysis inresposne to Crystallite size of ZG:RE^{3+} doped NPs

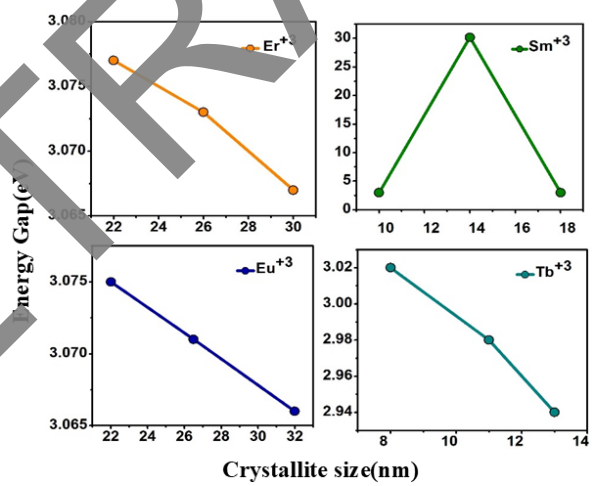

Figure 3. Variation of optical band gap energy (Eg), determined from UV–Vis Tauc plots, as a function of crystallite size for RE^{3+} = (Er^{3+}, Sm^{3+}, Eu^{3+}, and Tb^{3+})-doped ZG samples

The variation of optical band gap energy with crystallite size (Fig3)for RE^{3+} = (Er^{3+}, Sm^{3+}, Eu^{3+}, and Tb^{3+})-doped ZG samples, derived from UV–Visible absorption and Tauc analysis, reveals a clear size-dependent behavior. For the Er^{3+}, Eu^{3+}, and Tb^{3+}-doped systems, the band gap energy decreases systematically with increasing crystallite size, indicating

an inverse relationship between crystallite dimension and optical band gap. Specifically, in the Er^{3+}-doped samples, the band gap reduces from 3.077 eV to 3.067 eV as the crystallite size increases from 22 nm to 30 nm. A similar decreasing trend is observed for Eu^{3+}, from 3.075 eV to 3.066 eV with size increasing from 23 nm to 32 nm, and Tb^{3+}, from 3.02 eV to 2.94 eV with size increasing from 8 nm to 13 nm. This behavior can be attributed to the reduction of quantum confinement effects at larger crystallite sizes and the simultaneous increase in defect states or lattice strain induced by dopant incorporation, which introduce localized energy levels within the forbidden gap and effectively narrow the band gap. In contrast, the Sm^{3+}-doped system exhibits a non-monotonic variation, where the band gap initially increases and then decreases with crystallite size, suggesting a competing influence of crystallite growth and defect-mediated electronic structure modification. The overall correlation between crystallite size and band gap energy confirms that rare-earth doping not only alters the electronic structure through impurity level formation but also indirectly tunes optical properties via microstructural evolution. These results, in conjunction with the UV absorption analysis, demonstrate that controlled RE^{3+} incorporation enables effective band gap engineering in ZG through size-dependent and defect-assisted mechanisms, which is advantageous for tailoring materials for optoelectronic and photonic applications.

3.4 Energy Gap analysis inresposne to mol% of ZG:RE^{3+} doped NPs

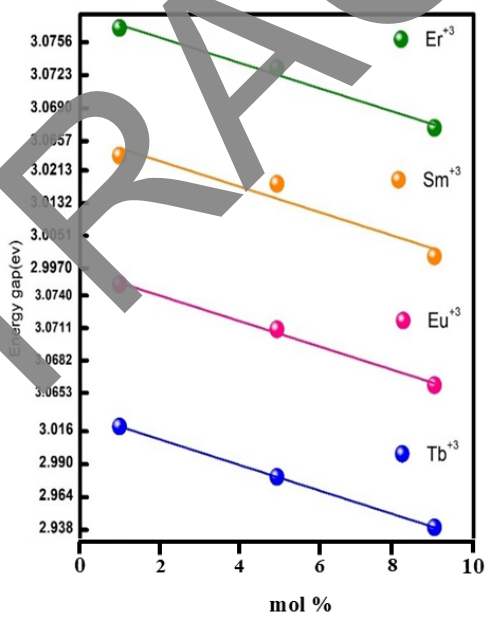

Figure 4. Variation of optical band gap energy (Eg), determined from UV–Vis Tauc plots, as a function of molar concentartion for RE^{3+} = (Er^{3+}, Sm^{3+}, Eu^{3+}, and Tb^{3+})-doped ZG samples

The figure illustrates the variation of optical band gap energy (Eg) as a function of dopant concentration(Fig4) (1, 5, and 9 mol%) for RE^{3+} = (Er^{3+}, Sm^{3+}, Eu^{3+}, and Tb^{3+}-doped ZG samples, where the band gap values were extracted from the UV–Visible absorption spectra using Tauc's relation for direct allowed transitions. A clear and systematic decrease

in Eg is observed with increasing rare-earth concentration for all dopants, indicating a progressive red shift of the absorption edge. In the Er^{3+}-doped samples, the band gap decreases from 3.076 eV (1 mol%) to 3.066 eV (9 mol%), while Sm^{3+} doping shows a reduction from 3.022 eV to 2.998 eV. Similarly, Eu^{3+}-doped ZG exhibits a gradual decrease from 3.074 eV to 3.065 eV, and Tb^{3+}-doped samples display a comparatively larger reduction from 3.016 eV to 2.938 eV with increasing dopant content.The monotonic decline in band gap energy with dopant concentration suggests that rare-earth incorporation effectively modifies the electronic structure of the ZG host lattice. This behavior can be attributed to dopant-induced lattice distortion due to ionic radius mismatch, which introduces strain and alters the periodic potential of the crystal. Additionally, higher dopant levels promote the formation of localized impurity states and defect levels—such as oxygen vacancies—within the forbidden gap. These intermediate states facilitate band tailing and reduce the effective energy separation between the valence and conduction bands, thereby narrowing the optical band gap. The stronger reduction observed in Tb^{3+}-doped samples may indicate enhanced defect formation or greater perturbation of the host electronic environment.

4 Summary

In this work, rare-earth (RE^{3+} = (Er^{3+}, Sm^{3+}, Eu^{3+}, and Tb^{3+})-doped $ZnGa_2O_4$ nanoparticles were successfully synthesized via an eco-friendly aloe-vera-assisted green combustion method, followed by calcination at 600^0C to enhance crystallinity. PXRD analysis confirmed the formation of a single-phase cubic spinel structure (Fd3m) without secondary impurity phases, demonstrating successful substitutional incorporation of RE^{3+} ions into the $ZnGa_2O_4$ lattice. Williamson–Hall analysis revealed nanoscale crystallite sizes and minimal, uniformly distributed microstrain, indicating that rare-earth doping does not disrupt the fundamental crystal symmetry but introduces controlled lattice distortion at the nanoscale.UV–Visible diffuse reflectance spectroscopy revealed strong absorption in the ultraviolet region associated with intrinsic band-to-band transitions and $O^{2-} \rightarrow RE^{3+}$ charge transfer processes, along with characteristic 4f–4f transitions of the dopant ions in the visible region. Tauc analysis confirmed a direct allowed transition for all compositions. A systematic red shift of the absorption edge and gradual narrowing of the optical band gap were observed with increasing dopant concentration, demonstrating effective band gap tuning through rare-earth incorporation.Furthermore, a clear correlation between crystallite size and optical band gap was established. For most dopants (Er^{3+}, Eu^{3+}, and Tb^{3+}), the band gap decreased with increasing crystallite size, reflecting reduced quantum confinement effects and enhanced defect-assisted band tailing. The concentration-dependent band gap reduction was attributed to dopant-induced lattice strain, impurity level formation, oxygen vacancy generation, and modification of the local electronic structure. Among the studied dopants, Tb^{3+} exhibited comparatively stronger band-gap narrowing at higher concentrations, indicating a more pronounced perturbation of the host electronic environment.Overall, the combined effects of controlled rare-earth substitution and nanoscale size modulation provide an efficient strategy for tailoring the electronic band structure of $ZnGa_2O_4$. The results highlight the potential of RE-doped $ZnGa_2O_4$ nanoparticles for advanced photonic, sensing, and optoelectronic applications where precise band gap engineering is essential.

References

[1]

[2] Lee, Mun Keun et al., Emission properties of Zinc Gallate nanophosphors. Journal of the Ceramic Society of Japan **126**, 382–388 (2018).

[3] Safeera, TA et al., Zinc gallate and its starting materials in solid state reaction route-A comparative study. Materials Chemistry and Physics **181**, 21–25 (2016).

[4] Jochan, Indu Treesa et al., Zinc Gallate Nanoparticles: A Multifunctional Material for Optoelectronic and Optical Limiting Applications. Journal of Alloys and Compounds 186302 (2026).

[5] Guo, Yuqiao et al., Surface chemical-modification for engineering the intrinsic physical properties of inorganic two-dimensional nanomaterials. Chemical Society Reviews **44**, 637–646 (2015).

[6] Rahman, Md Habibur et al., Understanding the role of rare-earth metal doping on the electronic structure and optical characteristics of ZnO. Molecular Systems Design & Engineering **7**, 1516–1528 (2022).

[7] Dwivedi, A et al., Multi-modal luminescence properties of RE3+ (Tm3+, Yb3+) and Bi3+ activated GdNbO4 phosphors—upconversion, downshifting and quantum cutting for spectral conversion. Journal of Physics D: Applied Physics **48**, 435103 (2015).

[8] Ghosh, Riti et al., Eu 3+ ions as a crystal-field probe for low-symmetry sites in doped phosphors–a case study: Eu 3+ at triclinic sites in Li 6 RE (BO 3) 3 (RE= Y, Gd), YBO 3 and ZnO and at trigonal sites in YAl 3 (BO 3) 4. Physical Chemistry Chemical Physics **25**, 25537–25551 (2023).

[9] Sood, Shagun et al., *Photonics* (MDPI, 2025) **12**, 454.

[10] Kharissova, Oxana V et al., Greener synthesis of chemical compounds and materials. Royal Society open science **6**, (2019).

[11] Claes, Romain et al., Establishing Doping Limits for ZnGa2O4 for Ultrawide-Band-Gap Semiconductor Applications. ACS Applied Materials & Interfaces **17**, 69659–69665 (2025).

[12] Soundar, R et al., Sustainable synthesis, electrochemical and photoluminescence investigations of ZnGa2O4: Sm3+ nanoparticles. Journal of Alloys and Compounds Communications 100150 (2025).

[13] Soundar, R et al., Spinel Cubic Tb3+ Doped ZnGa2O4 Nanoparticles for Display and High Energy Storage Device Applications. Journal of Molecular Structure 143913 (2025).

[14] Manjunatha, HC et al., Photonic and laser protection potential of rare-earth ions (Eu3+, Tb3+, Sm3+, Er3+, Dy3+) doped ZnGa2O4 nanoparticles synthesized via aloe vera combustion route. Materials Research Bulletin 114018 (2026).